Arabian Journal for Science and Engineering (2019) 44:305–313
https://doi.org/10.1007/s13369-018-3648-6

RESEARCH ARTICLE - CHEMISTRY

Fast and Fully Scalable Synthesis of Graphene Oxide from Cellulose by Catalytic Acid Spray Method (CAS)

Mahmoud Fathy[1] · Th. Abdel Moghny[1] · Mahmoud Ahmed Mousa[2]

Received: 20 May 2018 / Accepted: 19 November 2018 / Published online: 29 November 2018

Abstract
Graphene oxide (GO) characterized by high electrical conductivity and thermal stability can be considered as a single monomolecular graphite layer, containing numerous functional oxygen groups such as epoxide, carbonyl, carboxyl and hydroxyl groups. Therefore, in this work, we have come to produce high quantities of GO sheets by innovative, simple and hydrazine-free methods based on rice straw, using catalytic acid spray method (CAS) in the presence of cobalt silicate nanoparticle as a catalyst. The structure of graphene oxide was characterized by FTIR, Raman, HR-TEM and DLS. FTIR shows that GO comprises some efficient hydroxyl (OH), epoxy (cyclic ether), carboxyl and carbonyl groups. XRD shows that the interlayer spacing of GO prepared by our techniques is higher to some extent than the interlayer spacing of other GO produced by another processes. We can say that, GO sheets can be produced for various applications, in large quantities, high efficiency and low cost, by adjusting the parameters such as acid strength or catalytic doses used in the CAS method. Thereby, we can overcome the weak inter-bond between the GO sheets without cracking them.

Keywords Graphene · Catalyst · Spray · Interspacing · Lattices · Silica

1 Introduction

Graphene that consisted of single thin carbon sheet with a hexagonally packed lattice structure has attracted the attention of researchers in both basic and applied science fields [1,2]. Important of graphene oxide is attributed to the low cost of its production, its accessibility and the possibility of transferring it to graphene on a large scale. GO attracted the physicists due to its electronic behavior under magnetic field and at low temperature. GO's transform properties from microscopic-to-molecular scales have attracted considerable attention to current research effort [3].

In these days, GO can be produce on a large scale via graphene exfoliation using strong oxidizing agents. GO is often synthesized by chemical oxidation of natural graphene, although it can be prepared with electrochemical oxidation as an alternative route [4]. Fortunately there are many synthetic strategies to produce good quality in huge amounts of graphene oxide at actual cost [5].

Nevertheless, the isolated graphene oxide monolayer has received double attention, and within a few years the scientists will be able to verify on the properties of this new yet ancient two-dimensional material [6]. At present, Hummers' method was widely adopted to produce GO, but it still suffers from several flaw, such as toxic gas generation (NO_2, N_2O_4), residual nitrate and low yield. Graphene oxides exhibit significant differences of its characteristics depending on the synthesis method and on the oxidation degree [7–9].

As an example, we found that the temperature point of explosive exfoliation of graphene oxide prepared by Brodie method is very higher compared to such point of graphene oxide produced by Hummers method by difference up to 100° with the same heating rates [1]. Also, it is noted a large difference in the hydration and solvation properties of graphene oxides prepared by Brodie and Hummers, respectively [1]. Recently, using of a mixture of H_2SO_4 and $KMnO_4$ to cut long-standing carbon nanotubes leads to produce a microscopic flat strips of graphene oxides and a few wide carbon atoms that have edges "capped" by oxygen atoms (=O) or hydroxyl groups (−OH) [1].

✉ Mahmoud Fathy
fathy8753@yahoo.com

[1] Applications Department, Egyptian Petroleum Research Institute (EPRI), 1 Ahmed El-Zomer, Box. No. 11727, Nasr City, Cairo, Egypt

[2] Faculty of Science Benha University, Fred Nada Street, Banha, Egypt

Bottom-up or (Tang-Lau method) is another method for preparing graphene oxide, at which the sole source is glucose, and characterized by its safer, simpler controlling on the layer wideness, varying from monolayer to multilayers by regulating the growth factors, finally it is more environmentally friendly compared to the conventionally "top-down" method, which is prepared in the presence of very strong oxidizers [10–12].

Because the exact structure of GO is complicated to define, the previous studies indicated that GO is communicable aromatic lattice of graphene hindering by epoxides, alcohols, ketones and n carboxylic groups. Such hindering of the lattice is indicated by increasing the interlayer spacing to 0.335 nm and 0.625 nm for graphene and GO, respectively. On the other hand, naturally flake graphene is a mineral purified by removing of heteroatom contaminate and when oxidized we can get GO. Therefore, there is strong economic demand for the production of graphene oxide by an effective method and on a huge scale. The synthesis of GO has become necessary, and the chemical methods needed to be reconsidered with a new challenge and with the possibility to return the reduction of GO sp^3 to graphene by low cost as possible [13].

In this paper, we applied the catalytic acid spray method to produce graphene oxide from cellulose as a natural source. The new graphene oxide sheets were described by Raman, XRD and TEM analysis. We see that the simplicity of operation method and the precision of our techniques might give us a chance to produce GO in a large scale.

2 Material and Methods

2.1 Materials

The commercially available rice straw was utilized as a source to synthesize of cellulose. In addition, the chemicals delivered from the local suppliers such as sulfuric acid (H_2SO_4) 98%, cobalt nitrate (Co $(NO_3)_2$), sodium hydroxide (NaOH) and silica were used as they are without purifying.

2.2 Preparation of Silica Cobalt Nanocomposites Catalysis

Direct precipitation method was used typically by dissolved 16.2 g of cetyltrimethylammonium bromide (CTAB) in solution containing 145 ml of deionized water at 30 °C ([14]. After that, 8.21 ml of tetraethyl orthosilicate (TEOS) as silicon source and 32 ml of 30% NH_3 were then added drop wise and stirred vigorously for 12 h to hydrolyze TEOS with 0.5 g cobalt nitrate. The product obtained was filtered and dehydrated under vacuum at 40 °C overnight. To remove surfactant, the samples were annealed at 550 °C in air for 4 h, after that the MCM-41 (Mobil Composition of Matter No. 41) were then obtained [15].

2.3 Extraction of Amorphous Microcrystalline Cellulose

Hemicellulose fraction in rice straw was hydrolyzed with 1% (wt/wt) H_2SO_4 at 120 °C for 60 min to get into hydrolysate fraction as monomeric sugars. Then the resulted residue (amorphous microcrystalline cellulose) was exposed to the delignification process using mixture of 1.5% (wt/wt) NaOH and 0.5% (wt/wt) H_2O_2 at 120 °C for 60 min. During alkaline peroxide delignification process, lignin and silica present in the pretreated rice straw were moved into the black liquor [3].

2.4 Preparation of GO Nano-Sheets using CAS Method

0.1 g silica was putted in 100-ml round-bottom flask and 5 g amorphous microcrystalline cellulose then added and dosed by 5 ml concentrated H_2SO_4, then left for 10 min, after that, it was filtrated, washed with boiling water till pH 7 and kept in oven at 40 °C for 6 h as seen the preparation and mechanism of reaction in Fig. 1. The prepared carbon material was decanted in a flask with 0.01 g cobalt silicate nanoparticle and heated to 40 °C for 30 min to obtain agglomerated GO sheet. Then the agglomerated GO sheet was left to cool for 1 h, and GO sheets were dehydrated at 50 − 70 °C for 24 h to obtain exfoliated single-layer GO [16].

3 Result and Discussion

3.1 Infrared Spectra

FIIR of cellulose in Fig. 2 shows absorbance's at 3416[1] band that attributed to stretching of the O–H bond (hydroxyl groups) of cellulose. Furthermore, an increase is observed for the bands around 2900 cm^{-1} assigned to the C–H stretching, due to the presence of the CH− and CH_2 -groups of the cellulose and CH_3− of the cellulose. 1638, 1417, 1323, 1161, 1046, and 895 cm^{-1} attributed to C–H stretching of CH_2 and CH_3 groups.

The absorption band of secondary CH–OH and primary CH_2-OH has been moved from 3407 to 3423 cm^{-1} after basic treatment, this indicates on broken of hydrogen bonds in cellulose [27]. Furthermore, CH_2- bending peak was shifted from 1431 to 1419 cm^{-1}, which indicated on the splitting of hydrogen bonds of cellulose. The stretching's of methylene and −C−H groups are located at 2800– 3000cm^{-1} [17].

The FTIR of GO (Fig. 2) exhibits three characteristic peaks at 1300, 1710 and 3450 cm^{-1} for carboxylic acids

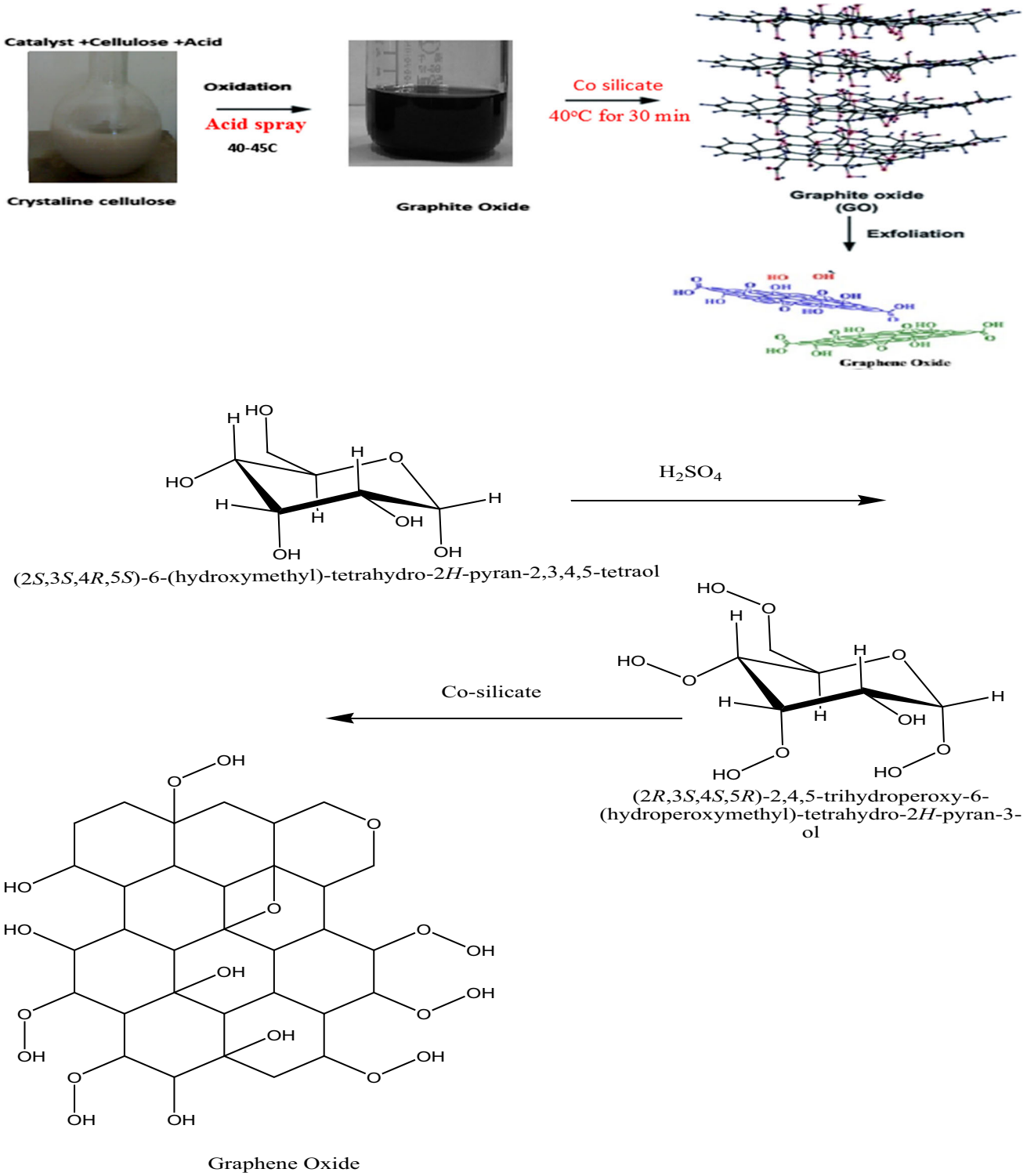

Fig. 1 The exfoliation of GO (200 nm) from microcrystalline cellulose by CAS method

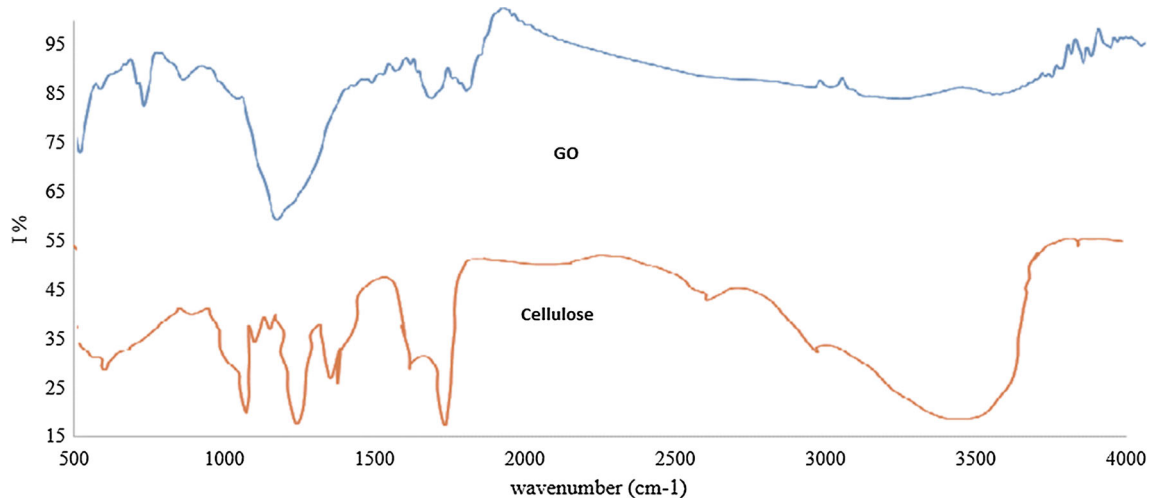

Fig. 2 FTIR of cellulose and prepared graphene oxide by CAS method

(COOH), carbonyl(CO) groups and hydroxyl groups(OH), respectively [18]. The bands at 1249 and 1134 cm^{-1} can be ascribed by asymmetric and symmetric S=O, respectively. This means that we successfully prepared GO having modified functional surface [19,20].

3.2 Analysis using XRD

Powder XRD analysis was applied to visualize the structural features of Co/silica catalysts and the prepared graphene sheets produced from cellulose by CAS method, and the results are displayed in Fig. 3. As shown from the XRD pattern of GO, the presence of inset distance between the layers has a significant consideration for describing the structural aspects of graphene. However, the (002) peak has been shifted to 13.05 ° for GO with a d-spacing value of 1.7997 nm [21] and that far from that appeared in other work (100) which is related to the (002) crystalline plane. Increasing of spacing between layers is indicated on the insertion of water moieties with oxygen functionalities of GO [22,23]. The considerable change of peak location is indicating on the great expansion of d-spacing due to the introducing of oxygen functionalities (such as C_OH, C_O_C, C_OOH) of graphite oxide. In reflection mode, the XRD pattern shows a strong (001) peak, indicating preferred orientation of graphene oxide basal planes parallel to the sample plane. The (001) *d*-spacing is 10 Å. Based on the (001) peak width, the crystallite size was determined using the Scherrer's technique and was found to be 60 Å in the [00l]-direction. Based on the obtained results, it is observed that the peaks are broader than that appear in other work results [24]. It may be due to the presence of carbon atom with higher surface area along with the composite materials [21].

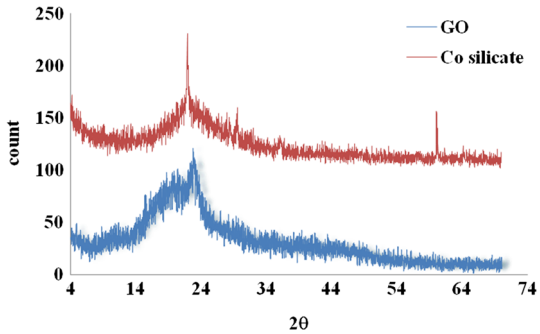

Fig. 3 XRD of cobalt silicate catalyst and graphene oxide that produced from cellulose by CAS method

We found also in Fig. 3 that Co/silica catalysts with a metal loading of 1 wt% were synthesized by Co $(NO_3)_2$ incipient wetness impregnation on silica to get catalysts with certain cobalt particle sizes. The XRD of hybrid Co/silica catalyst in Fig. 3 displays a characteristic reflection peak at 2 θ of 19 °, 31.3 °, 36.9 °, 44.8 °, 59.4 ° and 65.2 °,which indicate the plane (111), (220), (311), (222), (440), (422), (511) and (440), respectively [25], and this is indicated on the presence of Co_3O_4 in crystalline phase inside the catalyst sample, our suggestion is conceded with the studies done by [8,25,26].

In regular silica-supported catalysts, the Co_3O_4 particle size was decreased from 13.2 to 7.5 nm [27], taking in consideration that the particle size of hybrid catalysts was calculated using X-ray broadening method as described by Scherrer's equation, where the crystallite size of hybrid catalyst is promoted by 50 nm. These values were confirmed by HR-TEM measurements which also indicated particle size distributions [28].

As we seen from XRD pattern of Co/silica catalysts, the three intensive peaks are observed at 21, 29 and 60^0, corresponding to 002, 100, 101 and 004 reactions, respectively.

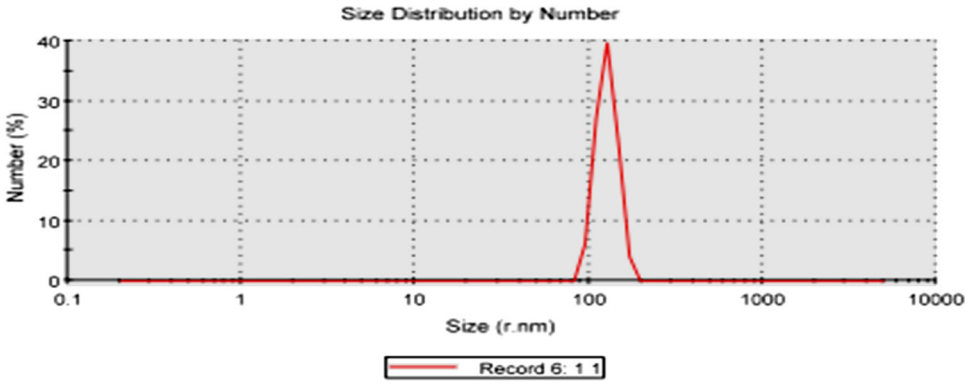

Fig. 4 The size distribution of graphene oxide by dynamic light scattering (DLS)

GO shows maximum broadband and sharp peak measured at 22.25 and 24.27, respectively [29].

We can suggested that the broadband appeared in XRD pattern of GO may be due to combination of graphene sheets with another layers produced as a result of different intercalation and de-intercalation stages of silicate content of catalyst or the cellulosic precursor materials. Also we found that the d-spacing values are ranging between 1.23 and 0.85 nm calculated using Bragg's equation [30].

3.3 Dynamic Light Scattering (DLS) Method

The size of new GO in an aqueous solution was measured using dynamic light scattering (DLS) method; DLS results displayed that the size of GO lays between 50 and 100 nm as presented in Fig. 4. Also it is shown that the hydrodynamic diameter of GO sheets is about 551.8 nm in the existence of water, which means that the GO particles produced from cellulose by CAS method and their dimension are somewhat higher than that of ordinary GO particles that are produced by another method because of the aggregation of GO fragments.

It is observable that the modification in the distribution size of GO sheets shows that CAS method not only represented as a strong oxidizing to synthesis graphene, but it was also functionalized the resulted surfaces of GO, leading to the increase in the Brownian motion rate afterward the reduction by chemical process [31,32].

3.4 Raman Spectroscopy

Raman spectroscopy was used to detect the quality of prepared graphene sheets and that is powerful candidate for quick and nondestructive inspection of many layers of graphene [33,34]. Raman spectroscopy of GO was used to verify the presence of graphene [35].

The spectrum of GO in Fig. 5 shows the intense peaks at 1348 cm^{-1} (D) and 1558 cm^{-1} (G). The G band that is existing in all sp2-hybridized carbon materials is due to stretching of the C–C bond; meanwhile, the D and D′ bands resulted from the disorder in the graphene flakes. The 2D band is slightly broader, between 2650 and 2700 cm^{-1} and very small that indicates very far sheets of GO [36]. The outcome results recommend that the prepared graphene sheets of graphene could be single sheet. Previous studies recommended that the graphene obtained by the reducing chemical method displays two distinguishing main peaks: G band at 1575 cm^{-1} and the D band at 1350 cm^{-1}. Here we detected that GO displays G band at 1558 cm^{-1} and D band at 1348 cm^{-1} separately (Fig. 5). The G band of GO showed a red shift from 1557 to 1558cm^{-1},and that known as regaining of carbon atoms in a hexagonal system. The intensity ratio IG/ID is used to assess the amount of defects in graphene and the in-plane crystallite. The intensity ratio (IG/ID) of prepared GO is 4 indicating on the appearance of disorder and some low defects in prepared GO comparing with (IG/ID) that of GOs produced by the other methods. This modification indicates that during the production process more SP^2 domains in graphene sheets were changed [37,38].

3.5 Electronic Absorption Spectra of Graphene Oxide

UV–vis absorption spectra of suspended GO in Fig. 6 show two bands at 270 nm which are assigned to p–p* of aromatic C–C bonds, and a shoulder at about 350 nm, can be recognized ton-π* transitions of C=O bonds [2,39,40].

The peaks are shifted to lower and higher wavelengths beside a decrease or disappearance of the peak due to n–p* transition which confirm the coordination catalyst with the carboxylic and OH groups on GO surface. Also, the spectrum obtained is in covenant with the previously reported results [38,41].

3.6 Thermal Analysis

Thermogravimetric curves of cellulose and GO in Fig. 7 show small initial brake near 100 °C may be to evaporate of retained moisture. The decomposition temperature of cellulose and GO started at 228 °C and 410 °C, respectively, our resulted agreement with that obtained by, who stated

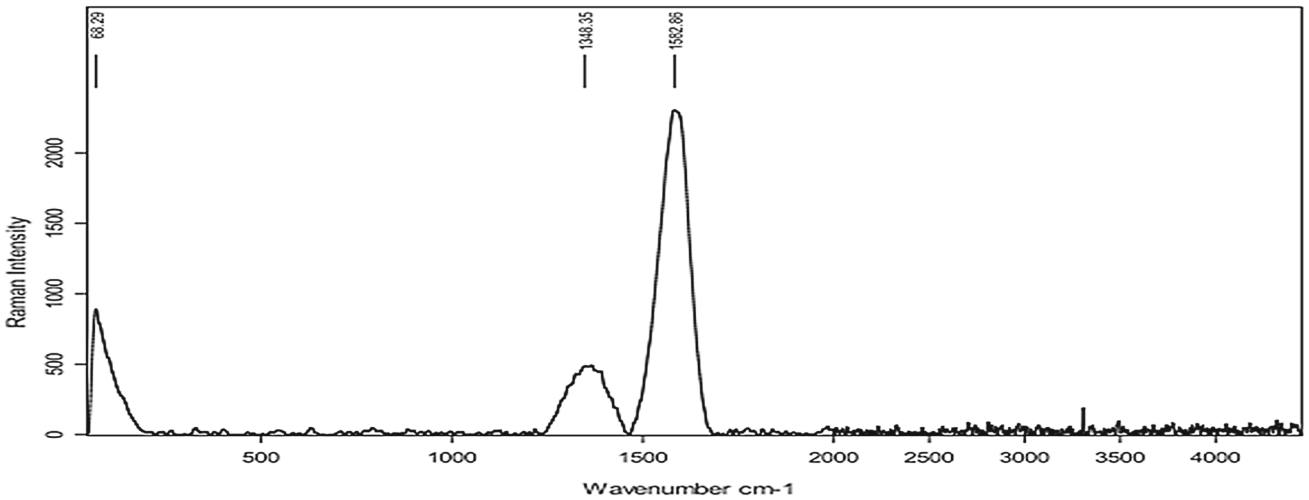

Fig. 5 Raman spectroscopy of graphene oxide that produced from cellulose

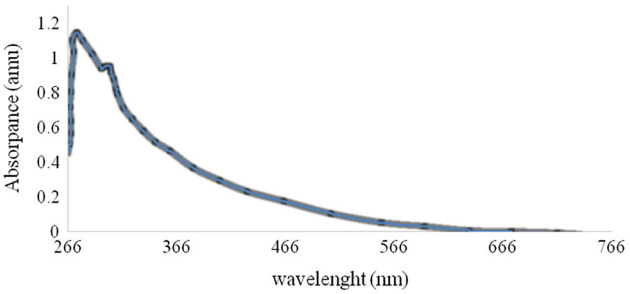

Fig. 6 UV–vis Spectrum of Graphene Oxide

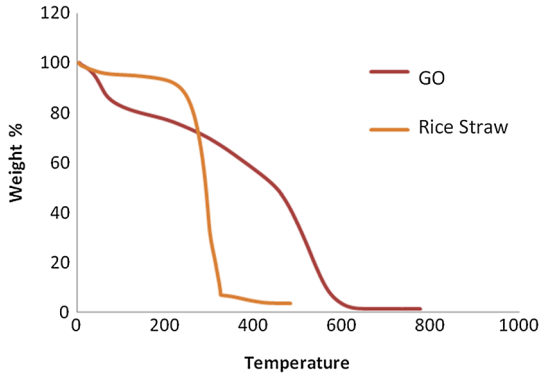

Fig. 7 TGA of cellulose and GO nanoparticles

that 50% of weight loss occurs at decomposition temperature of 300 °C and 450 °C for cellulose and GO, respectively [42,43].

The decomposition temperature decreasing trends inferred that the thermal stability of cellulose was lower than that of GO, which was probably due to partial hydrolysis and degradation of macromolecular cellulose during pretreatment. The higher degradation residues of GO proposed that some impurities from silica and the catalyst are involved in synthesis process and may be contributed to produce yield over 100% of some samples [33].

3.7 The Structure Analysis

As we discussed in this section, the structure of Co-silicate catalysis and GO sheets was illustrated by HR-TEM, SAED and EDX analyses. As seen from Fig. 8, the HR-TEM image of Co-silicate NPs indicated that the lattice spacing ranging is of ~50 nm and are distributed randomly anchored agglomerated onto each other.

The irregular spherical surface morphology observed might be due to the impregnation of the Co oxide into the silicate catalyst. The top right image of Fig. 8 indicates a lattice spacing of 0.691 nm, which could be ascribed to the (100) planes of magnetite (CoO). So we can say that through the production reaction, cobalt atoms migrate to the silica particle surface, creating a cobalt oxide epitaxial film [44]. In the future, such atomic information provides an important reference point for designing and engineering better Co-silicate catalyst [45].

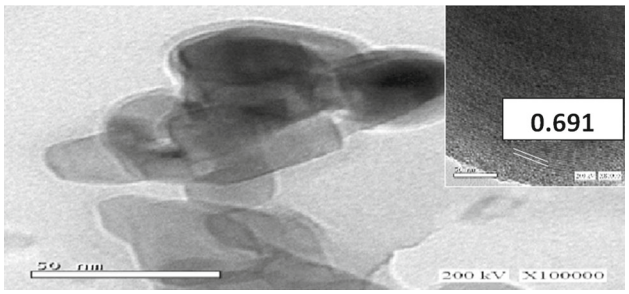

Fig. 8 HR-TEM of Co-silicate catalyst with lattices spacing image

HR-TEM images of the graphene oxide nanoparticles sheets in Fig. 9 show that the distance between graphene

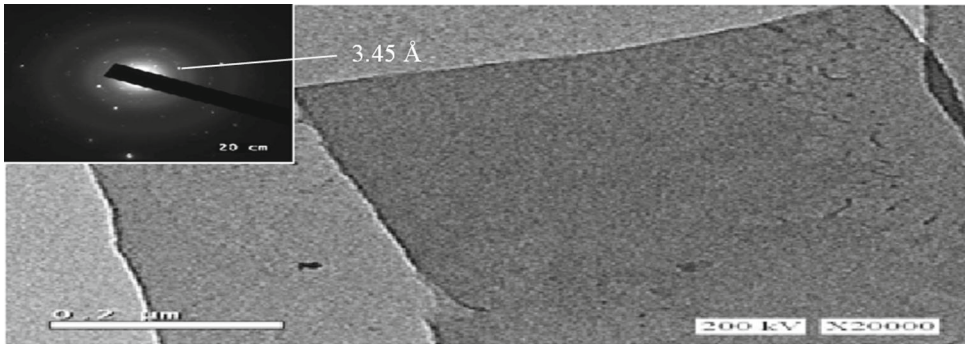

Fig. 9 HR-TEM and SAED of graphene oxide sheets

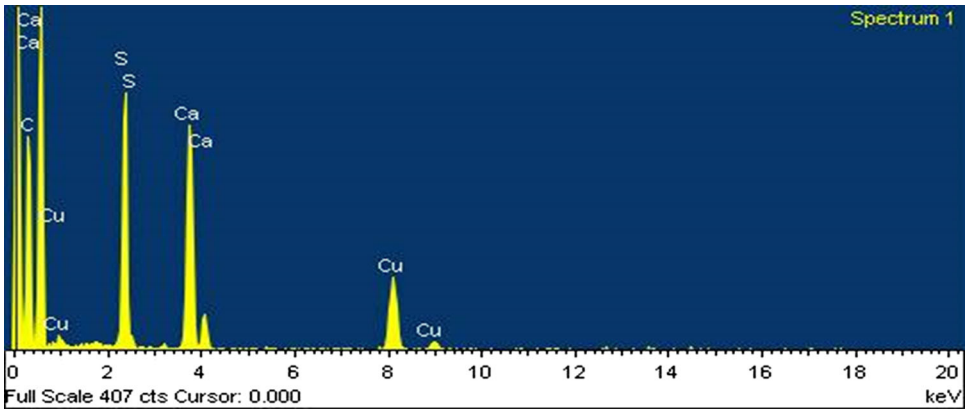

Fig. 10 EDX of graphene oxide sheets

oxide layers was about 1nm which is more than the interlayer distance of graphite, suggesting the growth of the few layers of GO on the surface of the Co-silicate nanoparticles.

Also, as seen in Fig. 9, graphene oxide flakes are separated from each others and indicating on the formation of single order of the GO sheets, also, the well-ordered hexagonal graphite lattices of mono-layered GO flakes are obviously indicating on the succeeding preparation of GO by CVD method. Moreover, there were nearly no silica nanoparticles separately from the GO, due to the strong interaction between the silica and GO [1,46,47].

The SAED analysis in the upper left image in Fig. 9 shows that NPs have hexagonal crystal structure and its lattice parameter is 3.45 Å and are higher than observed in other synthesis methods [48]. Taking into consideration, that the typical precision n of HR-TEM analysis is generally not exceeded than a few percent; therefore, the notable lattice margins can be attributed to the catalyst and the flat surface of GO, respectively .

EDX of GO sheets in Fig. 10 exhibited the existence of C, O, and Co elements, which means that the majority elements in GO are 80.59 wt% C and 19.98 wt% O, also, this confirmed that silica nanoparticels were homogeneously distributed in the GO, also, it is a further proof to the absence of any impurities in the sample [49].

3.8 Understanding the Chemical Structure of Graphene Oxide Monolayers

From one of the proposed graphene models that are shown in Fig. 11, we can see that the graphene sheet remains attained as a flat surface with a coronene armchair structure. Such structural was conformed previously by Martínez et al [29] and demonstrated experimentally by You et al [29]. As we know that the Raman spectroscopy is a possible and practical technique helping to identify the edge chirality of graphene and determine its crystal orientation, thereby, in Fig. 11, the presence of a regular array of epoxy groups (C–O–C) spread across on the graphene surface with a net molecular formula of C_2O gives an good experimental indication on the presence of hydrogen in graphite oxide. Accordingly, an important aspect of this model is that each graphene layer is distorted by the presence of functional groups and carbon atoms interact through sp^3 bonds. Thereby, we can assume that the prepared graphene oxide consisted of multiple graphene sheets bonding by oxygen above and below the individual graphene sheet. The FTIR and Raman spectra evidence on the trapping of water molecules between graphene layers, and consequently, the proposed model emphasized on the presence of interaction between the hydroxyl and carbonyl functional groups trapping in the distorted graphene sheets [50]. Also, they argued that the experimentally observed changes in the interlayer spacing in graphene oxide with humidity can be

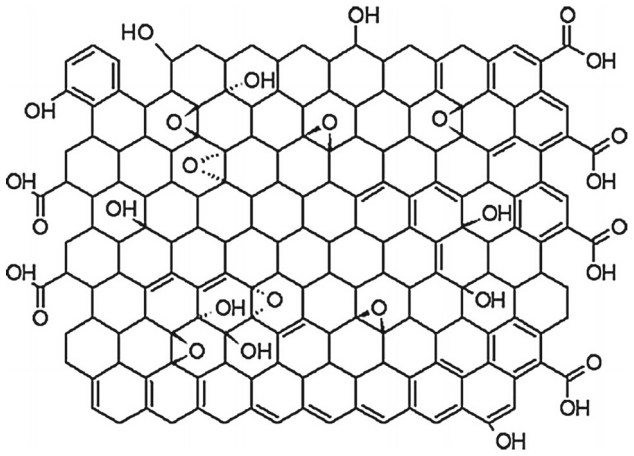

Fig. 11 Chemical structure of graphene oxide sheet with arbitrarily dispersed epoxy and hydroxyl groups, as well as, carboxyl groups alongside the edges

directly related to the ratio of hydroxyl-to-carbonyl groups, ranging from a completely dehydrated structure, C_8O_2, to a structure dominated by hydroxyl groups, $C_8(OH)_4$. While this model provides a possible range of structures based on water content, it is important to note that it still relies on a crystalline vision of prepared graphene oxide with a periodic arrangement of functional groups [50].

4 Conclusion

We presented a development simple chemical treatment technique at room temperature to synthesize water-soluble graphene by aqueous acid exfoliation of cellulose with Co-silicate as a catalyst. All the Raman spectroscopy, DLS and XRD confirmed the foundation of individual GO sheets having large interspacing. HR-TEM and EDX analyses revealed that GO has good regular structure, and little percentage of impurities is appeared during the production process. Our current findings offer an environmentally friendly and a profitable method for producing stable GO; this method can be adjusted for bulk production. According to our experience, this is the first example for CAS method to produce GO. Finally, we can announce that the CAS method is an efficient and simple method for producing high-yield and low-cost graphene suspensions.

References

1. Fathy, M.; et al.: Incorporation of multi-walled carbon nanotubes in microspheres used as anion exchange resin via suspension polymerization. Appl. Nanosci. **4**(5), 543–549 (2014)
2. Randviir, E.P.; Brownson, D.A.C.; Banks, C.E.: A decade of graphene research: production, applications and outlook. Mater. Today **17**(9), 426–432 (2014)
3. Ramzi, M.; El-Sayed, R.H.; Fathy, M.; Moghny, T.A.: Evaluation of scale inhibitors performance under simulated flowing field conditions using dynamic tube blocking test. Int. J. Chem. Sci. **14**(1), 16–28 (2016)
4. Farrag, A.E.H.A.; Moghny, T.A.; Gad, A.M.; Saleem, S.S.; Fathy, M.; Ahmed, M.A.: Removing of hardness salts from groundwater by thermogenic synthesis zeolite. SDRP J. Earth Sci. Environ. Stud. **1**, 109 (2016)
5. Farrag, A.E.H.A.; Moghny, T.A.; Gad, A.M.: SSSaleem, M Fathy, Abu Zenima synthetic zeolite for removing iron and manganese from Assiut governorate groundwater. Egypt. Appl. Water Sci. **7**, 3087 (2016). https://doi.org/10.1007/s13201-016-0435-y
6. Farrag, A.; et al.: Removing of hardness salts from groundwater by thermogenic synthesis zeolite. J. Hydrogeol. Hydrol. Eng. **5**(4), 9647 (2016). https://doi.org/10.4172/2325
7. Fathy, M.; Abdel Moghny, T.; Awad, A.E.; AbdElhamid, : Cation exchange resin nanocomposites based on multi-walled carbon nanotubes. Appl. Nanosci. **4**(1), 103–112 (2014)
8. Xu, J.; Wang, Y.; Hu, S.: Nanocomposites of graphene and graphene oxides: synthesis, molecular functionalization and application in electrochemical sensors and biosensors. A review. Microchim. Acta **184**(1), 1–44 (2017)
9. Lee, J.H.; et al.: Adsorption mechanisms of lithium oxides (LixO2) on N-doped graphene: a density functional theory study with implications for lithium-air batteries. Theor. Chem. Acc. **135**(3), 50 (2016)
10. Fathy, M.; et al.: Nano composites of polystyrene divinylbenzene resin based on oxidized multi-walled carbon nanotubes. Int. J. Modern Org. Chem **2**(1), 67–80 (2013)
11. Liang, K.; et al.: Preparation and microwave absorbing properties of graphene oxides/ferrite composites. Appl. Phys. A **123**(6), 445 (2017)
12. Xu, Z.: Graphene oxides in filtration and separation applications. In: Gao, W. (ed.) Graphene Oxide: Reduction Recipes, Spectroscopy, and Applications, pp. 129–147. Springer, Cham (2015)
13. Fathy, M.; et al.: Study the adsorption of sulfates by high cross-linked polystyrene divinylbenzene anion-exchange resin. Appl. Water Sci. **7**(1), 309–313 (2017)
14. El-Sayed, M.; Ramzi, M.; Hosny, R.; Fathy, M.; Abdel, T.: Moghny, Breakthrough curves of oil adsorption on novel amorphous carbon thin film. Water Sci. Technol. **73**(10), 2361–2369 (2016)
15. Fathy, M.; El-Sayed, M.; Ramzic, M.; Abdelraheem, O.H.: Adsorption separation of condensate oil from produced water using ACTF prepared of oil palm leaves by batch and fixed bed techniques. Egypt. J. Pet. **27**, 319 (2017)
16. Magdy, A.; Wassel, M.F.; Hosny, R.; Desouky, A.M.; Mahmod, A.M.: Study the removal of cupper ions from textile effluent using cross linked chitosan. In: 8th International conferences of Textile Research Division (2017)
17. Magdy, A.; Wassel, M.F.; Hosny, R.; Desouky, A.M.; Mahmod, A.M.; Abdelraheem, O.H.: Evaluation of chromium (Cr III) adsorption using modified chitosan from different pH aqueous solutions. In: 9th International Conference On Chemical and Environmental Engineering (2018)
18. Fathy, M.; Abdel Moghny, T.; Abdou, M.M.; El-Bellihi, A.-H.A.-A.: Study the adsorption of Ca (II) and Mg (II) on high cross linked polystyrene divinyl benzene resin. Int. J. Modern. Chem. **7**(1), 36–44 (2015)
19. Mahmoud Fathy, T.A.M.; Mousa, M.A.; ElBellihi, A.-H.A.-A.; Awadallah, A.E.: Sulfonated ion exchange polystyrene composite resin for calcium hardness removal. Int. J. Emerg. Technol. Adv. Eng. **5**(10), 20–29 (2015)
20. Fathy, M.; Moghny, T.A.; Mousa, M.A.; El-Bellihi, A.-H.A.-A.; Awadallah, A.E.: Synthesis of transparent amorphous carbon thin films from cellulose powder in rice straw. Arab. J. Sci. Eng. **42**, 225 (2016). https://doi.org/10.1007/s13369-016-2273-5

21. Rosaiah, P.; et al.: Synthesis of flower-like reduced graphene oxide-Mn3O4 nanocomposite electrodes for supercapacitors. Appl. Phys. A **124**(9), 597 (2018)
22. Ramzi, M.; et al.: Breakthrough curves of oil adsorption on novel amorphous carbon thin film. Water Sci Technol. **73**(10), 2361 (2016)
23. Fathy, M.; Moghny, T.A.; Mousa, M.A.; El-Bellihi, A.-H.A.-A.; Awadallah, A.E.: Absorption of calcium ions on oxidized graphene sheets and study its dynamic behavior by kinetic and isothermal models. Appl. Nanosci. **6**, 1105 (2016). https://doi.org/10.1007/s13204-016-0537-8
24. Bolagam, R.; Boddula, R.; Srinivasan, P.: Design and synthesis of ternary composite of polyaniline-sulfonated graphene oxide-TiO2 nanorods: a highly stable electrode material for supercapacitor. J. Solid State Electrochem. **22**(1), 129–139 (2018)
25. Nagarani, S.; et al.: Synthesis and characterization of binary transition metal oxide/reduced graphene oxide nanocomposites and its enhanced electrochemical properties for supercapacitor applications. J. Mater. Sci. Mater. Electr. **29**(14), 11738–11748 (2018)
26. Moghny, T.A.; et al.: Preparation of sorbent materials for the removal of hardness and organic pollutants from water and wastewater. World Acad. Sci. Eng. Technol. Int. J. Environ. Chem. Ecol. Geol. Geophys. Eng. **11**(5), 461–468 (2017)
27. Moghny, M.F.M.A.M.T.A.: Characterization and evaluation of amorphous carbon thin film (ACTF) for sodium ion adsorption. Appl. Water Sci. **7**, 4427 (2017). https://doi.org/10.1007/s13201-017-0588-3
28. Ali, A.; Bahadur Rahut, D.; Behera, B.: Factors influencing farmersx adoption of energy-based water pumps and impacts on crop productivity and household income in Pakistan. Renew. Sustain. Energy Rev. **54**, 48–57 (2016)
29. Ali, M.E.A.; et al.: Thin film composite membranes embedded with graphene oxide for water desalination. Desalination **386**, 67–76 (2016)
30. Ammar, A.I.; Kruse, S.E.: Resistivity soundings and VLF profiles for siting groundwater wells in a fractured basement aquifer in the Arabian Shield, Saudi Arabia. J. Afr. Earth Sci. **116**, 56–67 (2016)
31. Alvino, A.; Barbieri, G.: Vegetables of temperate climates: leafy vegetables A2 - Caballero, Benjamin. In: Finglas, P.M., Toldrá, F. (eds.) Encyclopedia of Food and Health, pp. 393–400. Academic Press, Oxford (2016)
32. Lin, Y.-C.; et al.: The synthesis and characterization of graphene oxides based on a modified approach. J. Therm. Anal. Calorim. **116**(3), 1249–1255 (2014)
33. Li, J.; et al.: Nanoscale zero-valent iron particles modified on reduced graphene oxides using a plasma technique for Cd(II) removal. J. Taiwan Inst. Chem. Eng. **59**, 389–394 (2016)
34. Singh, R.; Kumar, D.; Tripathi, C.C.: Concentration enhancement of liquid phase exfoliated graphene with addition of organic salts. Proc. Comput. Sci. **70**, 565–571 (2015)
35. Gupta, S.; Carrizosa, S.B.: Graphene-inorganic hybrids with cobalt oxide polymorphs for electrochemical energy systems and electrocatalysis: synthesis, processing and properties. J. Electr. Mater. **44**(11), 4492–4509 (2015)
36. Wang, K.: Synthesis of hydrophobic carbon nanotubes/reduced graphene oxide composite films by flash light irradiation. Front. Chem. Sci. Eng. **12**(3), 376–382 (2018)
37. Prince, J.A.; et al.: Ultra-wetting graphene-based membrane. J. Membr. Sci. **500**, 76–85 (2016)
38. Justh, N.; et al.: Thermal analysis of the improved Hummers' synthesis of graphene oxide. J. Therm. Anal. Calorim. **131**(3), 2267–2272 (2018)
39. Sun, W.; et al.: Synthesis of magnetic graphene nanocomposites decorated with ionic liquids for fast lead ion removal. Int. J. Biol. Macromol. **85**, 246–251 (2016)
40. Timofeeva, T.E.; et al.: The effect of temperature conditions during graphene oxide synthesis on humidity dependence of conductivity in thermally reduced graphene oxide. J. Struct. Chem. **59**(4), 799–805 (2018)
41. Khatmi Maab, N.Z.; Shokuhfar, A.; Ahmadi, S.: The effect of temperature and type of peroxide on graphene synthesized by improved Hummers' method. Int. Nano Lett. **6**(4), 211–214 (2016)
42. Zhu, Y.; et al.: Monolithic supermacroporous hydrogel prepared from high internal phase emulsions (HIPEs) for fast removal of Cu2+ and Pb2+. Chem. Eng. J. **284**, 422–430 (2016)
43. Jilani, A.; et al.: Graphene and its derivatives: synthesis, modifications, and applications in wastewater treatment. Environ. Chem. Lett. **16**, 1301 (2018)
44. Xue, X.; et al.: Synthesis of graphene oxide nanosheets for the removal of Cd(II) ions from acidic aqueous solutions. J. Taiwan Inst. Chem. Eng. **59**, 365–372 (2016)
45. Gunda, R.; Madireddy, B.S.; Dash, R.K.: Synthesis of graphene oxide and reduced graphene oxide using volumetric method by a novel approach without NaNO2 or NaNO3. Appl. Nanosci. **8**(4), 751–758 (2018)
46. Thiagarajan, K.; et al.: Synthesis of Ni3V2O8@graphene oxide nanocomposite as an efficient electrode material for supercapacitor applications. J. Solid State Electrochem. **22**(2), 527–536 (2018)
47. Hosny, R.; et al.: Treatment of the oily produced water (OPW) using coagulant mixtures. Egypt. J. Pet. **25**(3), 391–396 (2016)
48. Xu, K.; et al.: Synthesis of highly stable graphene oxide membranes on polydopamine functionalized supports for seawater desalination. Chem. Eng. Sci. **146**, 159–165 (2016)
49. Xu, X.; et al.: Design and fabrication of mesoporous graphene via carbothermal reaction for highly efficient capacitive deionization. Electrochim. Acta **188**, 406–413 (2016)
50. Stewart, D.A.; Mkhoyan, K.A.: Graphene oxide: synthesis, characterization, electronic structure, and applications. In: Raza, H. (ed.) Graphene Nanoelectronics: Metrology, Synthesis, Properties and Applications, pp. 435–464. Springer, Berlin (2012)